5. A. V. Lykov, Izv. Akad. Nauk SSSR, Énerg. Transport, No. 5 (1970).
6. P. V. Tsoi, Methods for Calculation of Individual Heat- and Mass-Transfer Problems [in Russian], Énergiya, Moscow (1971).
7. M. A. Mikheev and I. M. Mikheeva, Fundamentals of Heat Transfer [in Russian], Énergiya, Moscow (1977).
8. A. V. Lykov, Heat and Mass Transfer (Handbook) [in Russian], Energiya, Moscow [1971).
9. W. Predöhl, Kunststoffe, 61, No. 7 (1971).

NUMERICAL SIMULATION OF AN EXPLOSIVE PLASMA GENERATOR IN THE GASDYNAMIC APPROXIMATION

G. S. Romanov and V. V. Urban

UDC 533.6

A two-dimensional gasdynamic model of a plasma generator is proposed. A numerical solution of the problem is obtained, and peculiarities of the gasdynamic flow are considered. Results are compared with experiment.

The explosive plasma generator proposed by A. E. Voitenko is used to produce dense plasma and high-velocity plasma flows which convert a large portion of their energy into radiant energy. The generator (Fig. 1a) is a closed chamber in the form of a spherical segment, filled with the working gas. A metal plate driven by the explosion products moves toward the top of this segment, forcing the working gas into the tube. Compressed many times by the action of the shock wave, the gas is strongly accelerated along the device axis, with the mass velocity of the gas being close to the phase velocity of the motion of the point where plate and spherical segment join, and many times higher than the velocity of the plate motion. As a result, the gas is transformed into a plasma with parameters $T \sim 10^5$°K, $p \sim 10^{10}$ Pa, $N \sim 10^{27}$ m^{-3}. Directly upon exit from the tube the plasma occupies a small volume; then there occurs nonstationary ejection of a flare, whereupon the jet velocity may reach values of $\sim(40\text{-}90) \times 10^3$ m/sec, depending on the nature of the working gas and conditions in the tube [1-4]. The continuous spectrum radiation from the front of the jet has a flux density of $\sim 10^{10}$-10^{12} W/m^2 with a total light energy of $\sim 3 \cdot 10^5$ J/m^2 over an irradiation time on the order of tens of μsec [9]. These and a number of other desirable features of such a generator have stimulated the appearance of a large number of experimental studies in which both the gasdynamic and radiant characteristics of the plasma flow produced have been studied [1-10]; however, obvious difficulties have prevented study of the dynamics of the processes occurring within the device. As far as development of a theory of processes in the generator is concerned, we have only [3], in which certain considerations pertaining to the principle of device operation were set forth and estimates of plasma parameters made, together with [6], which presented certain calculated and experimental data. In [6] the flow in the generator compression chamber was assumed two-dimensional, while the flow of plasma into the tube, forming the directed flow, was assumed one-dimensional. Results were presented only for certain integral plasma parameters and shock-wave trajectories in the generator, and no data characterizing the development of gasdynamic processes were presented.

The present study is an attempt at direct numerical simulation of the gasdynamic processes in such a generator by indirect calculation of the nonstationary axisymmetric flow which develops throughout its entire volume. We will use the following formulation of the problem. At the initial moment t = 0 under the action of the explosion products the plate of mass M begins to move into the compression chamber (the spherical segment) at a velocity V, losing its kinetic energy to compression and acceleration of the working gas filling the segment in accordance with the expression

$$\frac{MV^2}{2} = E_{in} - \int_0^t \Delta p S U dt'. \quad (1)$$

V. I. Lenin Belorussian State University. Translated from Inzhenerno-Fizicheskii Zhurnal, Vol. 37, No. 5, pp. 859-867, November, 1979. Original article submitted January 15, 1979.

0022-0841/79/3705-1325$07.50

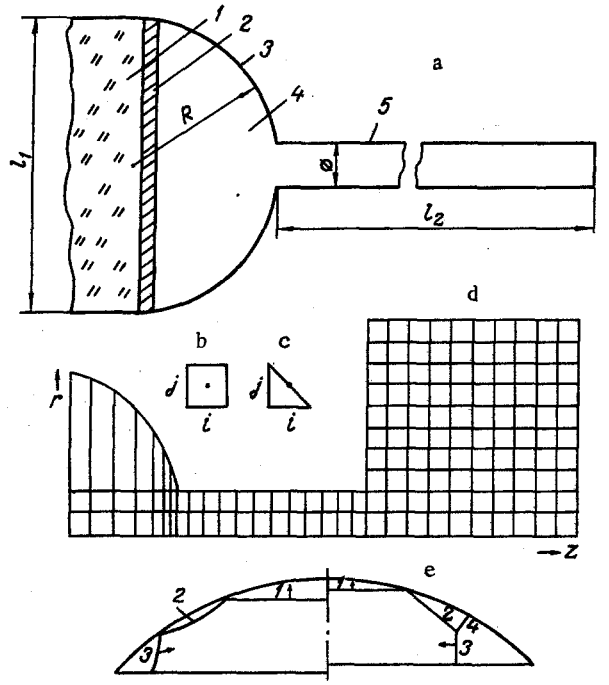

Fig. 1. a) Diagram of Voitenko's explosive generator: 1) explosive charge; 2) plate; 3) spherical segment; 4) working gas; 5) tube; l_1 = 0.1 m, l_2 = 0.2 m, R = 0.08 m, ⌀ = 0.023 m); b, c) different network cells; d) subdivision of computation region; e) shock-wave configuration within spherical segment.

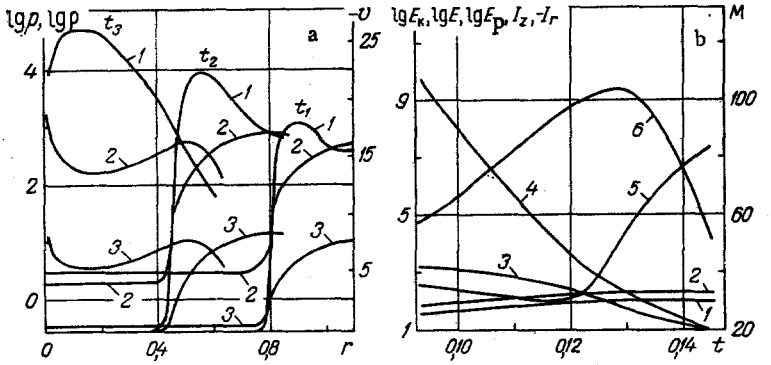

Fig. 2. a) Distribution of various quantities over plate radius: 1) radial gas velocity (-v); 2) pressure, log p; 3) density, log ρ at times t_1 = 0.1, t_2 = 0.115, t_3 = 0.132; b) time variation of integral quantities: 1) gas kinetic energy, log E_k; 2) total gas energy, log E; 3) plate kinetic energy, log E_p; 4) plate mass, M; 5) axial gas momentum, I_z; 6) radial gas momentum ($-I_r$).

According to the data of [6], the plate remains planar in the course of its motion, which allows us to avoid consideration of its interaction with the segment wall, and to determine the mass M for each moment of time from the area of the segment base at that time. Further, we neglect loss of gas energy due to friction and heat exchange with the walls, considering the gas to be nonviscous and not thermally conductive. We then obtain a system of equations describing the flow in Eulerian representation in a cylindrical coordinate system:

$$\frac{\partial \rho}{\partial t} + \operatorname{div}(\rho \mathbf{w}) = 0;$$

$$\frac{\partial \rho u}{\partial t} + \operatorname{div}(\rho u \mathbf{w}) + \frac{\partial p}{\partial z} = 0;$$

$$\frac{\partial \rho v}{\partial t} + \operatorname{div}(\rho v \mathbf{w}) + \frac{\partial p}{\partial r} = 0; \tag{2}$$

$$\frac{\partial \rho E}{\partial t} + \operatorname{div}(\rho E \mathbf{w}) + \operatorname{div}(p \mathbf{w}) = 0; \quad p = p(\rho, \varepsilon).$$

The initial data for the equation system (1), (2) is given at t = 0 by the values U = U_0, u = 0, v = 0, $\varepsilon = \varepsilon_0$, $\rho = \rho_0$. Boundary conditions on the immobile rigid walls and the axis of symmetry require the normal velocity component to tend to zero, $w_n = 0$, while on the boundary between plate and working gas, the normal velocities must be equal.

The equation of state of the medium $p = p(\rho, \varepsilon)$, obtained by solving the complete system of Saha equations by the method of [11], with numerical integration of the finite-difference energy equation of system (2) is used in the form of a network function in logarithmic variables. The values of log p in each cell of the computation network of the problem are found by linear interpolation from the nearest nodes of this function.

The integration region (Fig. 1d) is subdivided into an irregular network of cells of two types, centered as shown in Fig. 1b, c. Such a subdivision of the computation region permits use in the general case of only two types of special (boundary) calculation cells (and in the case considered only one special cell need be used) instead of the 12 which must be employed in the regular network of [12], significantly simplifying calculation in the presence of movable boundaries. The finite-difference equations for system (2) to first-order accuracy in the full cell (b) are analogous to the "coarse particle" method of [13], while for the partial cells (c) we have

$$u_{ij} = u^n_{ij} - (2p^n_{ij} - p^n_{i-\frac{1}{2},j}) \frac{\Delta t}{\Delta z_i \rho^n_{ij}}; \tag{3}$$

$$v_{ij} = v^n_{ij} - (2p_{ij} - p_{i,j-\frac{1}{2}}) \frac{\Delta t}{\Delta r_j \rho^n_{ij}}; \tag{4}$$

$$\tilde{v}^n_{ij} = \operatorname{sign}(v_{ij}) \frac{|u_{ij}|\beta + |v_{ij}|}{1+\beta^2}; \tag{5}$$

$$\tilde{u}^n_{ij} = \operatorname{sign}(u_{ij}) |\tilde{v}^n_{ij}| \beta; \tag{6}$$

$$\tilde{E}^n_{ij} = E^n_{ij} + (A_j p^n_{i-\frac{1}{2},j} u^n_{i-\frac{1}{2},j} + A_{j-\frac{1}{2}} p^n_{i,j-\frac{1}{2}} v^n_{i,j-\frac{1}{2}})/\rho^n_{ij}; \tag{7}$$

$$\rho^{n+1}_{ij} = \rho^n_{ij} + \begin{cases} \rho^n_{i-1,j} \tilde{u}^n_{i-\frac{1}{2},j} A_j; \ \tilde{u}^n_{i-\frac{1}{2},j} > 0 \\ \rho^n_{ij} \tilde{u}^n_{i-\frac{1}{2},j} A_j; \ \tilde{u}^n_{i-\frac{1}{2},j} < 0 \end{cases} + \begin{cases} \rho^n_{i,j-1} \tilde{v}^n_{i,j-\frac{1}{2}} A_{j-\frac{1}{2}}; \ \tilde{u}^n_{i,j-\frac{1}{2}} > 0, \\ \rho^n_{ij} \tilde{v}^n_{i,j-\frac{1}{2}} A_{j-\frac{1}{2}}; \ \tilde{v}^n_{i,j-\frac{1}{2}} < 0; \end{cases} \tag{8}$$

$$X_{ij} = \tilde{X}^n_{ij} \frac{\rho^n_{ij}}{\rho^{n+1}_{ij}} + \frac{1}{\rho^{n+1}_{ij}} \begin{cases} \tilde{X}^n_{i-1,j} \rho^n_{i-1,j} \tilde{u}^n_{i-\frac{1}{2},j} A_j; \ \tilde{u}^n_{i-\frac{1}{2},j} > 0 \\ \tilde{X}^n_{ij} \rho^n_{ij} \tilde{u}^n_{i-\frac{1}{2},j} A_j; \ \tilde{u}^n_{i-\frac{1}{2},j} < 0 \end{cases} + \frac{1}{\rho^{n+1}_{ij}} \begin{cases} \tilde{X}^n_{i,j-1} \rho^n_{i,j-1} \tilde{v}^n_{i,j-\frac{1}{2}} A_{j-\frac{1}{2}}; \ \tilde{v}^n_{i,j-\frac{1}{2}} > 0, \\ \tilde{X}^n_{ij} \rho^n_{ij} \tilde{v}^n_{i,j-\frac{1}{2}} A_{j-\frac{1}{2}}; \ \tilde{v}^n_{i,j-\frac{1}{2}} < 0, \end{cases} \tag{9}$$

where

$$X = \{u, v, E^{n+1}\}; \ \tilde{X}^n = \{\tilde{u}^n, \tilde{v}^n, \tilde{E}^n\}; \ \beta = \Delta z_i / \Delta r_j;$$

$$A_j = \frac{2 r_j \Delta t}{\left(r_j - \frac{\Delta r_j}{6}\right) \Delta z_i}; \quad A_{j-\frac{1}{2}} = \frac{2 r_{j-\frac{1}{2}} \Delta t}{\left(r_j - \frac{\Delta r_j}{6}\right) \Delta r_j}.$$

Values of quantities at the cell boundaries, $p^n_{i-\frac{1}{2},j}$; $p^n_{i,j-\frac{1}{2}}$; $u^n_{i-\frac{1}{2},j}$; $v^n_{i,j-\frac{1}{2}}$; $\tilde{u}^n_{i-\frac{1}{2},j}$; $v^n_{i,j-\frac{1}{2}}$, are determined by interpolation of the corresponding values at the cell centers:

$$p^n_{i,j-\frac{1}{2}} = \frac{p^n_{i,j-1}\Delta r_j + p^n_{ij}\Delta r_{j-1}}{\Delta r_j + \Delta r_{j-1}};\quad u^n_{i-\frac{1}{2},j} = \frac{u^n_{i-1,j}\Delta z_i + u^n_{ij}\Delta z_{i-1}}{\Delta z_i + \Delta z_{i-1}};$$

$$\tilde{v}^n_{i,j-\frac{1}{2}} = \frac{\tilde{v}^n_{i,j-1}\Delta r_j + \tilde{v}^n_{ij}\Delta r_{j-1}}{\Delta r_j + \Delta r_{j-1}};\ \text{etc.}$$

The velocities u^{n+1}_{ij} and v^{n+1}_{ij} are calculated by formulas similar to Eq. (5), (6).

The equation of plate motion in difference form is written as

$$U^{n+1} = \left[(U^n)^2 - \sum_j \frac{4\pi p^{n+1}_{1,j} r_j \Delta r_j}{M^{n+1}} U^n \Delta t\right]^{1/2}. \tag{10}$$

Calculation of each step in time is divided into several stages. In the first, plate motion occurs along the axis a distance Δz, and new values of Δ^{zi}, Δr_j, r_j, $r_{j\pm1/2}$, and plate area and mass are calculated. The gas is assumed immobile. In the second stage, neglecting mass flow across cell boundaries, we define intermediate values of the gasdynamic quantities $\tilde{u}^n_{ij}$, $\tilde{v}^n_{ij}$, $\tilde{E}^n_{ij}$ using Eqs. (3)-(7). Further, in the third stage, we consider passage of mass, momentum, and energy through cell boundaries and gas displacement under the action of the plate. Using Eqs. (8), (9), written with consideration of the boundary conditions, we calculate values of density, velocity components, and gas energy for the new time value. The pressure is found from a table of $p = p(\rho, \varepsilon)$ values. The fourth stage consists of definition of a new plate velocity with Eq. (10). With this stage the new time step is completed.

For the stability criterion of the finite-difference system we employ the standard Courant condition, according to which

$$\Delta t = k\,\frac{\min\{\Delta z_i,\ \Delta r_j\}}{\max\{(|w| + c)_{ij}\}}. \tag{11}$$

Upon approach of the plate to the boundary of a cell of the Eulerian computation grid $\Delta z_i \to 0$, and thus the time step $\Delta t \to 0$ [Eq. (11)], so that at $\Delta z_i = \Delta z_{min}$ the procedure of combining cells with small dimensions is performed so that the volume of the new cell is equal to the sum of the volumes of the two previous ones. The values of the gasdynamic quantities in the new cell are determined from the conditions of conservation of mass, momentum, and system energy. Plate motion within the tube is not considered, since its mass and velocity are already low by such time.

We will consider the results of a numerical solution for a device with measurements as indicated in Fig. 1a, which correspond to the experimental conditions of [9]. In accordance with [9] the plate mass $M_0 = 43.8\cdot10^{-3}$ kg, $U_0 = 6\cdot10^{-3}$ m/sec. The working gas used was neon with initial pressure $p_0 = 10^5$ Pa and density $\rho_0 = 8.95\cdot10^{-1}$ kg/m^3. The finite-difference equations corresponding to Eqs. (1), (2) with initial and boundary conditions were solved for dimensionless variables. The characteristic values of the dimensional variables in the problem were taken as length, $l_* = \varnothing = 2.3\cdot10^{-2}$ m; velocity, $w_* = 10^3$ m/sec; pressure, $p_* = 10^7$ Pa; density, $\rho_* = 10^{-1}$ kg/m^3. In this case $\varepsilon_* = 10^6$ J/kg; $M_* = 1.2\cdot10^{-4}$ kg; $E_* = 1.2\cdot10^2$ J. Figure 1d shows shock-wave configurations in the working chamber at successive moments in time, separated in intervals Δt (left, earlier; right, later). The shock wave generated by the plate 1 is reflected from the spherical segment wall in the form of wave 2, which in turn intersects with lateral wave 3, formed by intense expulsion of gas from the region near the junction of the plate and spherical segment. Initially the intersection of waves 2 and 3 is regular, then as a result of the increasing angle between wave 3 and the spherical segment surface it becomes irregular (Machlike) and a triple configuration develops because of departure of the intersection point from the wall and the appearance of wave 4 [14].

We note that the wave picture found in the calculation agrees with that described in [3], the only difference being that in the calculation we find the development of the lateral wave 3, which inhibits multiple reflection of wave 1 from the sides of the angle formed by the

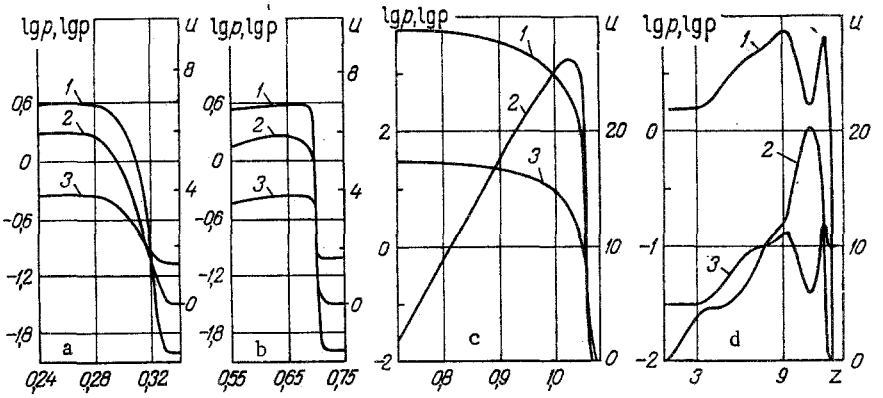

Fig. 3. Distribution of quantities over z axis: 1) gas pressure, log p; 2) axial gas velocity, u; 3) density, log p, at: a) t_1 = 0.04; b) t_2 = 0.093; c) t_3 = 0.138; d) t_4 = 0.6.

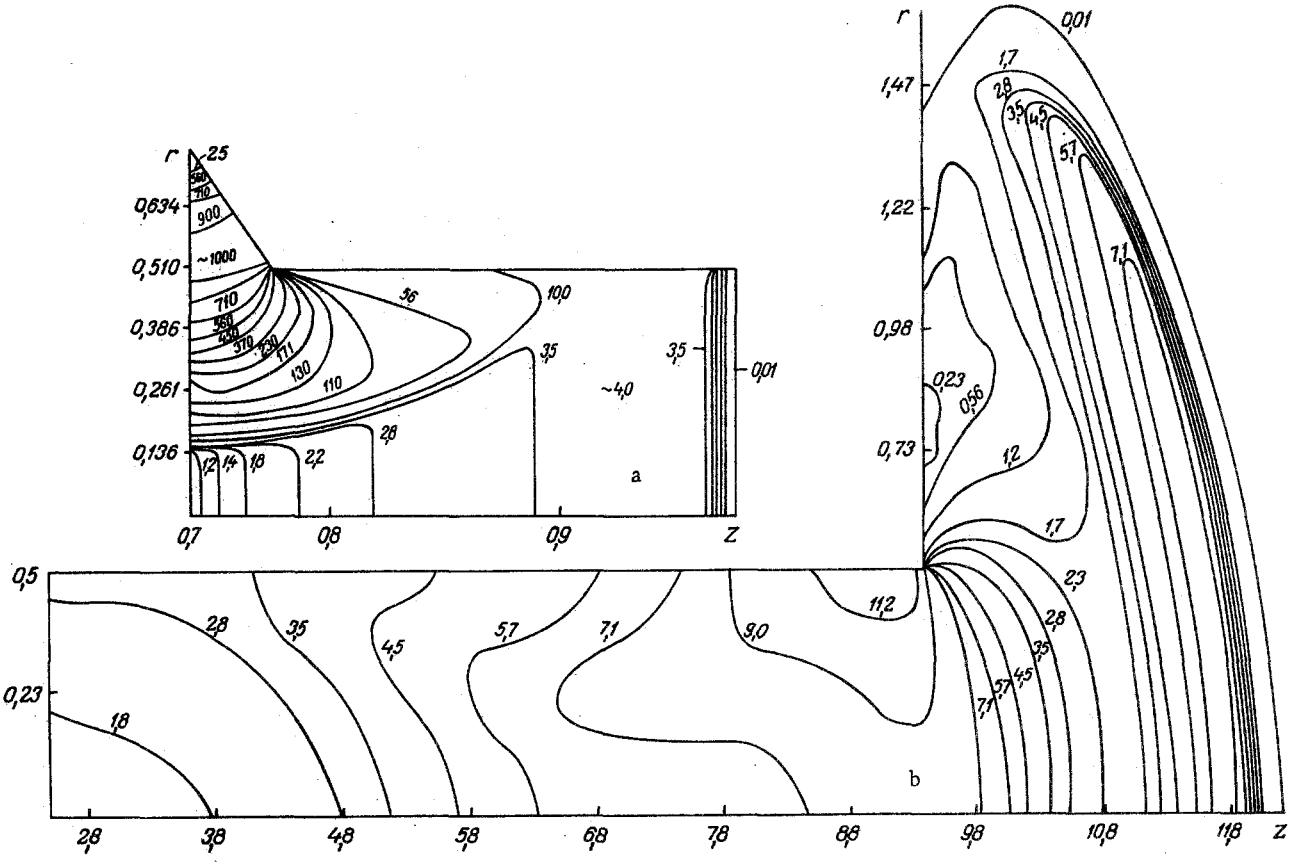

Fig. 4. Spatial pressure distribution at a) t_1 = 0.125; b) t_2 = 0.592.

segment surface and the plate. Beyond reflected wave 2 there occurs compression and partial braking of the gas in the direction of the axis. The greatest compression and radial velocity occur behind the front of lateral wave 3 (Fig. 2a). The increase in these parameters with approach of the plate to the end of the chamber is marked. The time t_3 in this figure corresponds to the beginning of the collision of gas flows on the axis and marked braking of the plate. The latter explains the reduction in $|v|$, p, and ρ inside the corner formed by the plate and chamber wall.

The behavior with time of the integral quantities characterizing motion from the moment of departure of the forward shock wave into the tube until the time the plate reaches the tube is shown in Fig. 2b. From the beginning of formation of discontinuities in the flow up to the time of complete exit of the flow into the tube, the kinetic and internal energies of the gas are practically equal in magnitude and increase with time. The total gas energy increases by a factor of 2.5 times, the kinetic energy of the plate drops by a factor of about 160, and its mass decreases by a factor of $\sim$5. We note that $\sim$5% of the plate energy is transferred to the plasma, which agrees with the experimental data of [9, 10]. The sharp increase in axial momentum at $t \sim 0.12$ begins because of departure of the lateral waves into the tube, and the fall in radial momentum at $t \sim 0.13$ is due to collision of these waves on the axis.

The direct shock wave propagating within the chamber changes parameters somewhat, following the plate velocity (Fig. 3a, b). At the beginning of gas flow collision on the axis and flow formation in the tube the velocity profile changes greatly (Fig. 3c), the form of the latter being characteristic of a moving jet. The time t_4 in this figure corresponds to departure of the jet into external space. The highest pressure and density values at this time are achieved at the beginning of the tube, then move to the head of the jet as the flare is expelled. As a result of the collision the pressure increases to several hundred thousand atmospheres, the density increases hundreds of times, and the temperature reaches hundreds of thousands of degrees. The pressure variation in the system for two different times (before collision of the lateral waves and after exit of the jet from the tube into the space beyond) is shown in Fig. 4a, b. It should be noted that the entire flow of the plasma jet within the tube is significantly non-one-dimensional, which invalidates the one-dimensional approximation used in [6]. After flow accumulation on the system axis at $t \sim 0.13$, as the tube fills with plasma, radial oscillatory motions are seen in the jet with a period of about 2 μsec, upon which the density and pressure rise in different manners on the axis and tube walls. It is interesting that the jet temperature remains practically constant ($\sim$6-7 eV) at all points while this occurs. The mean velocity of the forward front of the flow at the 10-cm section comprises 27 km/sec, which agrees well with the data of [9].

Thus, the results presented confirm the validity of the numerical model chosen, permitting its use for prediction of necessary conditions for production of optimal plasma parameters.

In conclusion, we note that the calculation of the problem was performed with a FORTRAN program on a Minsk-32 computer. To verify the reliability of the solution obtained various calculation grids were used, with 28 × 22, 56 × 44, and 112 × 88 cells along the radius and axis of the spherical segment, and 6, 12, and 24 cells along the tube radius. There was no significant change in the flow pattern with change from the coarser to the finer grid, but the propagation velocity of the lateral shock wave did differ. This can be explained by the dependence of the gas mass velocity in the wave on the accuracy with which the chamber wall surface is approximated. Satisfactory convergence of the calculation results was achieved even with the intermediate-size grid.

The authors thank R. I. Soloukhin for his support, and A. E. Viotenko, A. A. Deribas, and V. I. Kirko for their suggestions, because of which this study was commenced.

NOTATION

T, temperature; p, pressure; N, number of gas particles per unit volume; **w** gas mass velocity vector with components $w_z = u$ and $w_r = v$; z, axial coordinate; r, radial coordinate t, time; E, total specific energy of gas; ε, specific internal energy; ρ, density; V, plate velocity; E_{in}, initial plate energy; M, plate mass; S, plate area; Δp, pressure difference between left and right sides of plate; Δt, Δz, Δr, time and space steps; $k < 1$, Courant number; c, velocity of sound in the gas. Indices: 0, initial value; *, characteristic dimensional quantities; i, j, grid cell indices along z and r; n, number of time step; ($\sim$), symbol denoting intermediate values of gasdynamic variables in a time layer.

LITERATURE CITED

1. A. E. Voitenko, Dokl. Akad. Nauk SSSR, 158, No. 6 (1964).
2. A. E. Voitenko, I. Sh. Model', and I. S. Samodelov, Dokl. Akad. Nauk SSSR, 169, No. 3 (1966).
3. A. E. Voitenko, Zh. Prikl. Mekh. Tekh. Fiz., No. 4 (1966).
4. A. E. Voitenko, Zh. Tekh. Fiz., 36, No. 1 (1966).

5. A. E. Voitenko, E. P. Matochkin, and A. F. Fedulov, Prib. Tekh. Éksp., No. 2 (1970).
6. B. H. Crowley and H. D. Glenn, in: Proc. Seventh Int. Shock Tube Symp., I. I. Glass (editor), Univ. Toronto Press, Toronto (1970), p. 314.
7. H. D. Glenn and B. H. Crowley, J. Appl. Phys., 41, No. 10 (1970).
8. H. D. Glenn and B. H. Crowley, J. Appl. Phys., 42, No. 13 (1971).
9. Yu. N. Kiselev and B. D. Khristoforov, Fiz. Goreniya Vzryva, No. 1 (1974).
10. A. E. Voitenko and V. I. Kirko, Fiz. Goreniya Vzryva, No. 6 (1975).
11. G. S. Romanov and L. K. Stanchits, Dokl. Akad. Nauk BSSR, 15, No. 3 (1971).
12. Yu. M. Davydov, Zh. Vychisl. Mat. Mat. Fiz., 11, No. 4 (1971).
13. O. M. Belotserkovskii and Yu. M. Davydov, Zh. Vychisl. Mat. Mat. Fiz., 11, No. 1 (1971).